

General theory for super-sensitive dual-wavelength phase metrology: error-free unwrapping and signal-to-noise ratio

MANUEL SERVIN,* MOISES PADILLA, AND GUILLERMO GARNICA

Centro de Investigaciones en Optica A. C., 37000 Leon Guanajuato, Mexico.

*mservin@cio.mx

Abstract: From 1971 to 2012 dual-wavelength optical-metrology used only the demodulated low-sensitivity phase-difference of two close-sensitive fringes. Dual-wavelength phase-metrology that additionally uses the phase-sum was first reported by Di et al. in 2013 [28]; this was an important step to increase the phase-accuracy in optical metrology. This and its derived papers however do not offer mathematical analysis for signal-to-noise ratio (SNR) for the phase-difference and phase-sum. Neither provide the mathematical analysis for unwrapping the phase-sum without errors. Here a general theory for super-sensitive two-wavelength phase-metrology is given. In particular mathematical analysis and formulas for SNR and error-free phase-unwrapping for two-wavelength metrology is provided. We start by phase-demodulating two close-sensitivity fringes by phase-shifting algorithms (PSAs). We then calculate their phase-difference and their phase-sum; the phase-difference is assumed non-wrapped. However the phase-sum is highly wrapped, super-sensitive and has much higher SNR. Spatial phase unwrapping for a highly discontinuous phase-sum is precluded. However as we show, it is possible to unwrap the noisy phase-sum from the noisier phase-difference without errors. We apply this super-sensitive phase-metrology theory to profilometry allowing us to obtain super-sensitive height measurements. To the best of our knowledge the mathematical analysis and formulas herein presented for the SNR and error-free unwrapping have not been reported before.

08 June 2017, Centro de Investigaciones en Optica (CIO).

OCIS codes: (120.0120) Instrumentation, measurement, and metrology; (100.2650) Fringe analysis; (120.6650) Surface measurements, figure.

References and links

1. K. J. Gasvik, *Optical Metrology*, 3th ed., (John Wiley & Sons, 2002).
2. M. Servin, J. A. Quiroga, and M. Padilla, *Interferogram Analysis for Optical Metrology, Theory Algorithms and Applications* (Wiley-VCH, 2014).
3. J. C. Wyant, "Testing aspherics using two-wavelength holography," *Appl. Opt.* **10**, 2113–2118 (1971).
4. C. Polhemus, "Two-wavelength interferometry," *Appl. Opt.* **12**, 2071–2074 (1973).
5. Y. Y. Cheng and J.C. Wyant, "Multiple-wavelength phase-shifting interferometry," *Appl. Opt.* **24**, 804–807 (1985).
6. Y. Y. Cheng and J.C. Wyant, "Two-wavelength phase shifting interferometry," *Appl. Opt.* **23**, 4539–4543 (1984).
7. R. Onodera and Y. Ishii, "Two-wavelength interferometry that uses a Fourier-transform method," *Appl. Opt.* **37**, 7988–7994 (1998).
8. J. Kühn, T. Colomb, F. Montfort, F. Charrière, Y. Emery, E. Cucho, P. Marquet, and C. Depeursinge, "Real-time dual-wavelength digital holographic microscopy with a single hologram acquisition," *Opt. Express* **15**, 7231–7242 (2007).
9. K. Falaggis, D. P. Towers, and C. E. Towers, "Multiwavelength interferometry: extended range metrology," *Opt. Lett.* **34**, 950–952 (2009).
10. T. Kakue, Y. Moritani, K. Ito, Y. Shimozato, Y. Awatsuji, K. Nishio, S. Ura, T. Kubota, and O. Matoba, "Image quality improvement of parallel four-step phase-shifting digital holography by using the algorithm of parallel two-step phase-shifting digital holography," *Opt. Express* **18**, 9555–9560 (2010).
11. C. Wagner, W. Osten, and S. Seebacher, "Direct shape measurement by digital wavefront reconstruction and multiwavelength contouring," *Opt. Eng.* **39**, 79–85 (2000).

12. D. Abdelsalam and D. Kim, "Two-wavelength in-line phase-shifting interferometry based on polarizing separation for accurate surface profiling," *Appl. Opt.* **50**, 6153–6161 (2011)
13. J. Li, L. G. Hasebrook, and C. Guan, "Optimized two-frequency phase-measuring-profilometry light-sensor temporal-noise sensitivity," *J. Opt. Soc. Am. A* **20**, 108-115 (2003).
14. E. H. Kim, J. Hahn, H. Kim, B. Lee, "Profilometry without phase unwrapping using multi-frequency and four-step phase-shift sinusoidal fringe projection," *Opt. Express* **17**, 7818-7830 (2009).
15. K. Liu, Y. Wang, D. L. Lau, Q. Hao, L. G. Hasebrook, "Dual-frequency pattern scheme for high-speed 3-D shape measurement," *Opt. Express* **18**, 5229-5244 (2010).
16. Y. Xu, S. Jia, X. Luo, J. Yang, Y. Zhang, "Multi-frequency projected fringe profilometry for measuring objects with large depth discontinuities," *Opt. Comm.* **288**, 27-30 (2013).
17. T. Liu, C. Zhou, Y. Liu, S. Si, Z. Lei, "Deflectometry for phase retrieval using a composite fringe," *Opt. Applicata* **94**, 451-461 (2014).
18. Y. Xu, S. Jia, Q. Bao, H. Chen, J. Yang, "Recovery of absolute height from wrapped phase maps for fringe projection profilometry," *Opt. Express* **22**, 16819 (2014).
19. W. Zhang, X. Lu, L. Fei, H. Zhao, H. Wang, and L. Zhong, "Simultaneous phase-shifting dual-wavelength interferometry based on two-step demodulation algorithm," *Opt. Lett.* **39**, 5375–5378 (2014).
20. J. Long, J. Xi, M. Zhu, W. Cheng, R. Cheng, Z. Li, Y. Shi, "Absolute phase map recovery of two fringe patterns with flexible selection of fringe wavelengths," *Appl. Opt.* **53**, 1794-1801 (2014)
21. J. M. Huntley and H. Saldner, "Temporal phase unwrapping algorithm for automated interferogram analysis," *Appl. Opt.* **32**, (1993).
22. H. O. Saldner and J. M. Huntley, "Temporal phase unwrapping: application to surface profiling of discontinuous objects," *Appl. Opt.* **36**, 2770-2775 (1997).
23. G. Pedrini, I. Alexeenko, W. Osten, H. J. Tiziani, "Temporal phase unwrapping of digital hologram sequences," *Appl. Opt.* **42**, 5846-5854 (2003).
24. M. Servin, J. M. Padilla, A. Gonzalez, and G. Garnica, "Temporal phase-unwrapping of static surfaces with 2-sensitivity fringe-patterns," *Opt. Express* **23**(12), 15806-15815 (2015).
25. M. Servin, M. Padilla, G. Garnica, and A. Gonzalez, "Profilometry of three-dimensional discontinuous solids by combining two-steps temporal phase unwrapping, co-phased profilometry and phase-shifting interferometry," *Opt. Laser Eng.* **87**, 75-82 (2016).
26. A. Papoulis, *Probability, Random Variables and Stochastic Processes*, 4th ed. (McGraw Hill, 2000).
27. K. Creath, "Step height measurement using two-wavelength phase-shifting interferometry," *Appl. Opt.* **26**(14), 2810-2816 (1987).
28. J. Di, W. Qu, B. Wu, X. Chen, J. Zhao, and A. Asundi, "Dual wavelength digital holography for improving the measurement accuracy," *Proc. SPIE* **8769**(19), G1-G6 (2013).
29. J. Di, J. Zhang, T. Xi, C. Ma, and J. Zhao, "Improvement of measurement accuracy in digital holographic microscopy by using dual-wavelength technique," *J. Micro/Nanolith. MEMS MOEMS* **14**(4), 041313 (Oct–Dec 2015).
30. C. Zuo, L. Huang, M. Zhang, Q. Chen, A. Asundi, "Temporal phase unwrapping algorithms for fringe projection profilometry: A comparative review," *Opt. Laser Eng.* **85**, 84–103 (2016).
31. J. Xiong, L. Zhong, S. Liu, X. Qiu, Y. Zhou, J. Tian, and X. Lu, "Improved phase retrieval method of dual-wavelength interferometry based on a shorter synthetic-wavelength," *Opt. Express* **25** (7) 7181-7191 (2017).
32. M. M. Servin, M. Padilla, and G. Garnica, "M. Servin, M. Padilla, and G. Garnica, "Extended depth-range profilometry using the phase-difference and phase-sum of two close-sensitivity projected fringes," arXiv:1704.04662 [physics.optics] (2017).

1. Introduction

Here we start by presenting the well known concept of synthetic lambda interferometry concept. Wyant used two close laser-wavelengths $\{\lambda_1, \lambda_2\}$ to test optical surfaces with a synthetic wavelength of $\Lambda_D = \lambda_1 \lambda_2 / |\lambda_1 - \lambda_2|$ [3]. Given that $\lambda_1 \approx \lambda_2$, the wavelength Λ_D is much longer than either $\{\lambda_1, \lambda_2\}$, *i.e.* $\Lambda_D \gg \{\lambda_1, \lambda_2\}$. The wavelength Λ_D is obtained by the difference $\varphi_D = \varphi_1 - \varphi_2$; being $\{\varphi_1 = (2\pi / \lambda_1)w, \varphi_2 = (2\pi / \lambda_2)w\}$, and $w(x, y)$ the wavefront under test. Double-wavelength phase-metrology was improved by Polhemus [4] and later on by Cheng [5,6] using digital phase-shifting algorithms (PSA). Afterwards Onodera et al. used Fourier phase-demodulation for profiling structures with long equivalent-lambda depth size [7]. Unfortunately, the demodulated phase was over-smoothed due to over filtered diffraction orders [7]. This in turn was followed by a large number of double-wavelength Fourier and PSA demodulation methods in such diverse applications as double-wave holographic

microscopy [8], extended range optical metrology [9], two-step digital holography [10], multiwavelength extended-range contouring [11], and two-wavelength surface profiling [12]. Dual-wavelength optical metrology using $\varphi_D = \varphi_1 - \varphi_2$ has also been applied to holography, fringe-projection profilometry and contouring [13-20]. These methods have been called among other, two-frequency profilometry [13], profilometry without phase unwrapping [14], dual-frequency shape measurement [15], large-depth discontinuous objects profilometry [16], deflectometry of composite fringe phase retrieval [17], absolute-height fringe-projection profilometry [18], dual-wavelength two-steps phase-shifting demodulation [19], two fringe patterns absolute-phase recovery [20]. Even though these methods [3-20] were applied to different optical phase-metrology experiments, all of them share the same mathematical background just described. These authors referred their techniques as extended-range, absolute-phase measurement, phase-metrology without phase-unwrapping or direct shape measurement [3-20]. Finally we comment that the paper by Katherine Creath [27] (mentioned by one reviewer) also use just the phase-difference φ_D in his paper. Creath do not mention the possibility of using the phase-sum $\varphi_2 + \varphi_1$ in his phase-metrology technique [27].

Therefore from 1971 [3] until 2012, dual-wavelength optical metrology was synonymous of demodulating two close-sensitive phases $\{\varphi_1, \varphi_2\}$ ($\varphi_1 \approx \varphi_2$) for obtaining the non-wrapped phase-difference $(\varphi_2 - \varphi_1) \in (-\pi, \pi)$. However in 2013 Di et al. [28] computed for the first time, the phase-sum $\varphi_S = \varphi_2 + \varphi_1$ to obtain higher sensitivity and higher SNR phase measurements. As 2017, both $\varphi_D = \varphi_2 - \varphi_1$ and $\varphi_S = \varphi_2 + \varphi_1$ for phase metrology has been published (in peer reviewed journals) by: Di et al. [28,29] (2013 and 2015) and Xiong et al. [31] (2017). And by Servin et al. in the arXiv.org [32], not knowing the existence of [28,29,31]. However searching in Google Scholar, the paper [28] has been cited just twice [29,31], so this paper is hardly known even today, four years later from its publication. This is unfortunate because we consider that [28] is an important leap forward in double-wavelength phase-metrology. That is because the phase-sum is far more sensitive than the phase-difference $\varphi_S = G\varphi_D$; being $G \gg 1.0$. And as we mathematically prove here, their SNR between $\{\varphi_S, \varphi_D\}$ is also much higher $\text{SNR}(\varphi_S) = G^2 \text{SNR}(\varphi_D)$.

On the other hand, Servin et al. [24,25], and afterwards Xiong et al. [31] showed that a higher sensitive phase may be unwrapped directly from a lower-sensitive non-wrapped one. Di et al. dealt only with continuous wavefronts $w(x, y)$ so they could unwrap φ_S spatially [28,29]. Finally a reviewer called our attention to Zuo et al. [30], but this paper only unwraps $\varphi_D = \varphi_2 - \varphi_1$ (Eqs. (7)-(8)-(10) in [30]); they do not mention $\varphi_S = \varphi_2 + \varphi_1$.

Here we present a new results not presented in [28,29,31]. These are

- Mathematical analysis and a closed-form formula to obtain error-free unwrapping for the noisy phase-sum $\varphi_S + n_S$ directly from the noisy phase-difference $\varphi_D + n_D$.
- Mathematical analysis and closed-form formula for the SNR for noisy phase-sum $\varphi_S + n_S$ and phase-difference $\varphi_D + n_D$.

Finally we stress that $\varphi_S = \varphi_2 + \varphi_1$ has a higher sensitivity than either $\{\varphi_1, \varphi_2\}$ (super-sensitivity). We thank a reviewer for calling our attention to the recent work by Di et al. [29], and by using Google Scholar we found the two additional works which use $\varphi_S = \varphi_2 + \varphi_1$ [28,31].

The plan of this paper is as follows: section 2 reviews the state of the art in two-wavelength phase-metrology up to mid 2017. Section 3 we demodulate two close-sensitivity phases $\{\varphi_1, \varphi_2\}$, from which we compute $\varphi_D = \varphi_2 - \varphi_1$ and $\varphi_S = \varphi_1 + \varphi_2$. In section 4, we

mathematically analyze the SNR for $\{\varphi_s, \varphi_D\}$. In section 5, we give a close-form formula for error-free unwrapping the noisy $\varphi_1 + \varphi_2$ from the noisy $\varphi_2 - \varphi_1$. In section 6 we use fringe-projection profilometry to exemplify our two-wavelength phase-metrology theory. In section 7 we show that $\varphi_1 + \varphi_2$ has about twice the sensitivity than a single high-carrier fringe-pattern. Finally in section 8 we draw some conclusions.

2. State of the art in two-wavelength optical metrology

As mentioned, during 1971-2012 dual-wavelength phase-metrology used only $\varphi_D = \varphi_2 - \varphi_1$ from two close-sensitive phases $\{\varphi_1, \varphi_2\}$; being $\varphi_D \in (-\pi, \pi)$ [3-27]. In 2013 Di et al. [28] first used the higher-sensitive $\varphi_s = \varphi_2 + \varphi_1$ for dual-wavelength phase-metrology; this was an important leap forward in phase-precision in phase-metrology [28].

Let us consider two close-wavelengths $\lambda_1 \approx \lambda_2$ (close-sensitivity) fringe patterns as,

$$\begin{aligned} I_1(x, y, \Delta) &= a(x, y) + b(x, y) \cos \left[\frac{2\pi}{\lambda_1} w(x, y) + \Delta \right]; \\ I_2(x, y, \Delta) &= a(x, y) + b(x, y) \cos \left[\frac{2\pi}{\lambda_2} w(x, y) + \Delta \right]. \end{aligned} \quad (1)$$

Where $a(x, y)$ is the background; $b(x, y)$ the contrast; $w(x, y)$ the measuring wavefront, and Δ a piston phase. From Eq. (1) we may find two synthetic-wavelengths $\{\Lambda_D, \Lambda_S\}$ as,

$$\begin{aligned} \Lambda_D &= \frac{\lambda_1 \lambda_2}{|\lambda_1 - \lambda_2|}; & \text{for } \varphi_1 - \varphi_2 &= \left(\frac{2\pi}{\lambda_1} - \frac{2\pi}{\lambda_2} \right) w = \frac{2\pi}{\Lambda_D} w; \\ \Lambda_S &= \frac{\lambda_1 \lambda_2}{|\lambda_1 + \lambda_2|}; & \text{for } \varphi_1 + \varphi_2 &= \left(\frac{2\pi}{\lambda_1} + \frac{2\pi}{\lambda_2} \right) w = \frac{2\pi}{\Lambda_S} w. \end{aligned} \quad (2)$$

The wavelength Λ_D is longer than either $\{\lambda_1, \lambda_2\}$, or $\Lambda_D \gg \{\lambda_1, \lambda_2\}$. In contrast, Λ_S is shorter than $\{\lambda_1, \lambda_2\}$; or $\Lambda_S \approx \lambda_1 / 2$ for $\lambda_2 = (1 + \varepsilon)\lambda_1$; $\varepsilon \approx 0$.

Given that $\varphi_s = G\varphi_D$ ($G \gg 1.0$), the phase-sum $\varphi_s^w = W(\varphi_s)$ is highly wrapped ($W(x) = \text{Arg}[\exp(ix)]$). However φ_s^w may be unwrapped from φ_D by temporal phase-unwrapping, but it would need at least G intermediate sensitive wrapped-phases [21-23]. To solve this Servin et al. [24,25] developed the 2-sensitivity phase-unwrapper,

$$\varphi_s = G\varphi_D + W \left[\varphi_s^w - G\varphi_D \right]; \quad \{ \varphi_D \in (-\pi, \pi), (\varphi_s - G\varphi_D) \in (-\pi, \pi) \}. \quad (3)$$

This formula [24,25] predates the page-long algorithm in [31], and unwraps φ_s^w directly from $\varphi_D \in (-\pi, \pi)$. This is the status in dual-wavelength phase-metrology as mid 2017.

3. Synthetic phase-difference and phase-sum estimations

Using the fringe-patterns in Eq. (1), and using the least-squares M -step PSA we demodulate our fringes obtaining the analytic signals [2],

$$\begin{aligned}
A_1(x, y)e^{i\varphi_1(x, y)} &= \sum_{m=0}^{M-1} I_1(x, y, m\Delta) e^{im\Delta}, \\
A_2(x, y)e^{i\varphi_2(x, y)} &= \sum_{m=0}^{M-1} I_2(x, y, m\Delta) e^{im\Delta}; \quad \Delta = 2\pi / M.
\end{aligned} \tag{4}$$

Then the following products are computed,

$$A_1 e^{i\varphi_1} [A_2 e^{i\varphi_2}]^* = A_1 A_2 e^{i[\varphi_1 - \varphi_2]}; \quad A_1 e^{i\varphi_1} [A_2 e^{i\varphi_2}] = A_1 A_2 e^{i[\varphi_1 + \varphi_2]}. \tag{5}$$

Obtaining,

$$\begin{aligned}
\varphi_D &= \frac{2\pi}{\Lambda_D} w; & \Lambda_D &= \frac{\lambda_1 \lambda_2}{|\lambda_1 - \lambda_2|}; \\
\varphi_S^W &= W \left[\frac{2\pi}{\Lambda_S} w \right]; & \Lambda_S &= \frac{\lambda_1 \lambda_2}{|\lambda_1 + \lambda_2|};
\end{aligned} \tag{6}$$

Where $W(x) = \text{Arg}[\exp(ix)]$. Note that $\varphi_S^W = W[\varphi_1 + \varphi_2]$ is highly wrapped and super-sensitive (beyond the optical range) while $\varphi_D \in (-\pi, \pi)$. Finally the sensitivity between $\{\varphi_S, \varphi_D\}$ is,

$$G = \frac{\varphi_S}{\varphi_D} = \frac{\lambda_1 + \lambda_2}{|\lambda_1 - \lambda_2|} = \frac{\Lambda_D}{\Lambda_S}, \tag{7}$$

That is, $\varphi_S(x, y)$ is (Λ_D / Λ_S) times more sensitive than $\varphi_D(x, y)$. This result although implicit in [28,29,31], was not explicitly stated as we do here. The SNR and error-free unwrapping for $\varphi_S(x, y)$ are tightly tied to the sensitivity increase G .

4. SNR between the phase-sum and phase-difference

In practice the demodulated phases $\{\varphi_1, \varphi_2\}$ are corrupted by white noise $\{n_1, n_2\}$ [2] as,

$$\begin{aligned}
\varphi_1(x, y) &\rightarrow \varphi_1(x, y) + n_1(x, y); \\
\varphi_2(x, y) &\rightarrow \varphi_2(x, y) + n_2(x, y).
\end{aligned} \tag{8}$$

Where $\{n_1, n_2\}$, ($n_2 \neq n_1$) are samples of a Gaussian random process [2,26]. The fields $\{n_1, n_2\}$ have zero average and variance $\sigma^2 = E\{n_1\} = E\{n_2\}$; being $E\{\cdot\}$ the ensemble average [26]. Then the phase-difference and phase-sum are,

$$\begin{aligned}
\varphi_D &= \varphi_2 - \varphi_1 = \left(\frac{2\pi}{\Lambda_D} \right) w + n_2 - n_1; \\
\varphi_S &= \varphi_2 + \varphi_1 = \left(\frac{2\pi}{\Lambda_S} \right) w + n_2 + n_1.
\end{aligned} \tag{9}$$

In a Banach space, $(1/A_\Omega) \iint |f|^2 d\Omega$ represents the average-energy or power of f ; being A_Ω the area of well-defined fringes Ω . As a consequence the SNR for $\{\varphi_D, \varphi_S\}$ are,

$$\begin{aligned} \text{SNR}(\varphi_D) &= \frac{\text{Signal Power}}{\text{Noise Power}} = \frac{\left(\frac{2\pi}{\Lambda_D}\right)^2 \iint_{(x,y) \in \Omega} |w|^2 d\Omega}{\iint_{(x,y) \in \Omega} |n_2 - n_1|^2 d\Omega}; \\ \text{SNR}(\varphi_S) &= \frac{\text{Signal Power}}{\text{Noise Power}} = \frac{\left(\frac{2\pi}{\Lambda_S}\right)^2 \iint_{(x,y) \in \Omega} |w|^2 d\Omega}{\iint_{(x,y) \in \Omega} |n_2 + n_1|^2 d\Omega}. \end{aligned} \quad (10)$$

Assuming $\{n_1, n_2\}$ ergodic and stationary, the noise-power of $\{n_2 - n_1, n_2 + n_1\}$ are equal [26] so the SNR gain between $\varphi_S(x, y)$ and $\varphi_D(x, y)$ is,

$$\frac{\text{SNR}(\varphi_1 + \varphi_2)}{\text{SNR}(\varphi_1 - \varphi_2)} = \left(\frac{\Lambda_D}{\Lambda_S}\right)^2 = G^2. \quad (11)$$

Thus, the super-sensitive phase $\varphi_S(x, y)$ has G^2 higher SNR than $\varphi_D(x, y)$. So it is much better use $\varphi_S(x, y)$ instead of just $\varphi_D(x, y)$. As far as we know, this result has not been published before, in particular [28,29,31] do not contain any SNR mathematical analysis.

5. Error-free phase-unwrapping for discontinuous phase-sum

Here we unwrap the noisy $\varphi_S^W = W[\varphi_1 + \varphi_2 + n_S]$ from noisy $\varphi_D = \varphi_1 - \varphi_2 + n_D$ without errors. The high gain $G \gg 1.0$ translates into noise limitations for error-free unwrapping for φ_S^W . Here we are assuming small phase-noise *i.e.* $\{|n_S| \ll \pi, |n_D| \ll \pi\}$.

For the noisy $(\varphi_D + n_D)$ and $(\varphi_S^W + n_S)$ our temporal unwrapping formula is [24, 25],

$$\varphi_S + n_S = G(\varphi_D + n_D) + W[(\varphi_S^W + n_S) - G(\varphi_D + n_D)]; \quad W[x] = \text{Arg}(e^{ix}). \quad (12)$$

The conditions for this phase-unwrapper to work properly are (reported in [24,25]),

$$(\varphi_D + n_D) \in (-\pi, \pi), \quad \text{and} \quad [\varphi_S + n_S - G(\varphi_D + n_D)] \in (-\pi, \pi). \quad (13)$$

Substituting the noiseless sensitivity relation $\varphi_S - G\varphi_D = 0$ into the second condition,

$$(n_S - Gn_D) \in (-\pi, \pi); \quad G = \frac{\Lambda_D}{\Lambda_S}. \quad (14)$$

This noisy signal must reside within $(-\pi, \pi)$ to unwrap $\varphi_S^W + n_S$ without errors. This last condition is a new result not reported in [24,25], neither in [28-32].

The most important fact to take note here is the product Gn_D ($G \gg 1.0$). Therefore we must keep n_D as low as possible by using many-steps PSAs. And as we said, this useful result has not been reported before [1-32].

6. Application example to super-resolution fringe-projection profilometry

Here we exemplify the general theory for dual-wavelength super-sensitive phase-metrology using two examples from 3D profilometry. These profilometry examples fully agree with the three previous experiments that use the phase-sum in other phase-metrology areas [28,29,31].

Digital fringe-projection profilometry has been known for many years [1]. A set up for three-dimensional (3D) profilometry of solids is shown in Fig. 1.

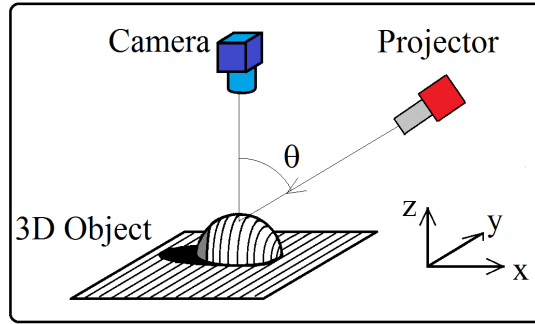


Fig. 1. Schematic of a fringe-projection profilometer. The digitizing solid is a sphere segment and θ is the sensitivity angle of this profilometer.

The mathematical model for the fringes $I_1(x, y)$ and $I_2(x, y)$ taken by the CCD camera are,

$$\begin{aligned} I_1(x, y, m) &= a(x, y) + b(x, y) \cos \left[u_1 \tan(\theta) h(x, y) + u_1 x + \frac{2\pi}{4} m \right]; \\ I_2(x, y, m) &= a(x, y) + b(x, y) \cos \left[u_2 \tan(\theta) h(x, y) + u_2 x + \frac{2\pi}{4} m \right]; \quad m = \{0.1.2.3\}. \end{aligned} \quad (15)$$

Where $h(x, y)$ the solid's height and θ the sensitivity angle (Fig. 1); the carriers $\{u_1, u_2\}$ are in radians/pixel. The angle (θ) is fixed and small to avoid large self-occluding shadows. The upper limit for $\{u_1, u_2\}$ is the Nyquist rate of π radians/pixel. However, here we are not using very-high carriers because the fringes would be hardly observable. The sensitivity gain is,

$$G = \frac{\varphi_s}{\varphi_D} = \frac{u_1 + u_2}{|u_1 - u_2|}. \quad (16)$$

All previous results apply just by substituting $\Lambda_D / \Lambda_S \rightarrow (u_1 + u_2) / |u_1 - u_2|$.

6.1 A calibrating spherical metallic cap

The spherical metallic cap in Fig. 2 is used as calibrating solid. This is a regular photography, not a three-dimensional (3D) digital rendering.

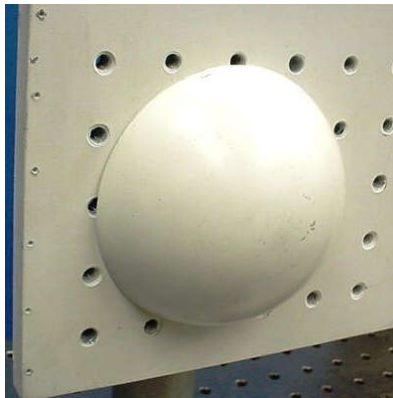


Fig. 2. Regular digital photograph of a calibrating spherical metallic cap..

In Fig. 3 we show the two close spatial-frequencies (close phase-sensitivities) linear-fringes projected on this spherical object. In the upper row of Fig. 3, we have projected linear-fringes with spatial-frequency $u_1 = 2\pi/7$ radians/pixel, while in the lower row the fringes have a carrier of $u_2 = 2\pi/6$ radians/pixel.

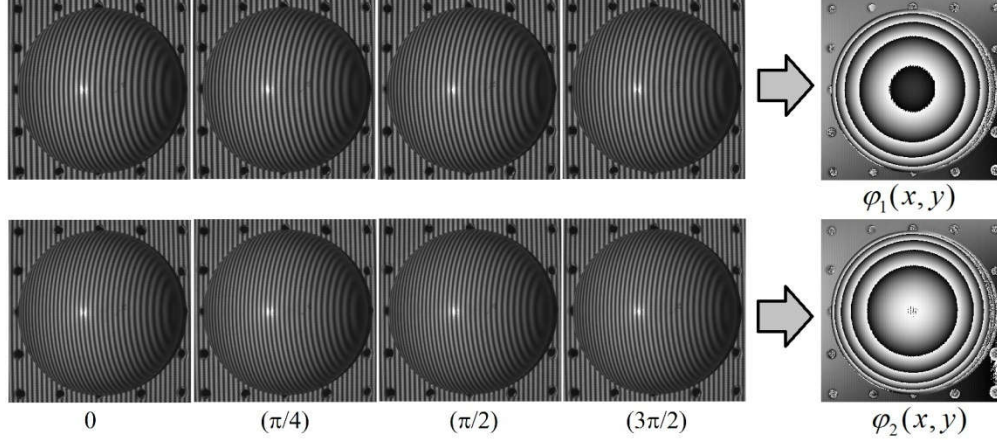


Fig. 3. A spherical segment illuminated by linear fringes and their phase demodulation. The phase-shifting among the fringe-patterns are $\{0, \pi/4, \pi/2, 3\pi/2\}$. The upper row has lower phase-sensitivity fringes than the lower row. The right column shows the demodulated wrapped phases.

Figure 4 shows the phase-subtraction (upper row) and the phase-addition (lower row) of the two demodulated phases in Fig. 4. The sensitivity gain G is then given by,

$$G = \frac{u_1 + u_2}{|u_1 - u_2|} = \frac{(2\pi/6 + 2\pi/7) \text{ Radians / Pixel}}{|2\pi/6 - 2\pi/7| \text{ Radians / Pixel}} = 13, \quad (17)$$

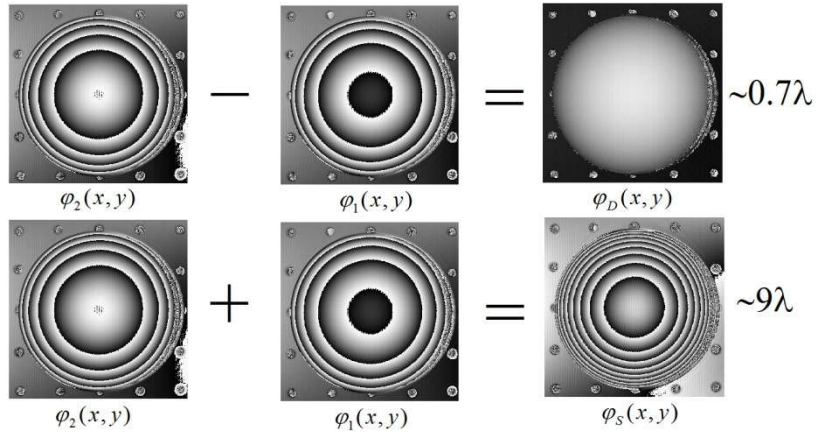


Fig. 4. The upper row shows the phase-difference while the lower row the phase-sum. The phase difference has about 0.7 lambda sensitivity and non-wrapped. The phase-sum is however wrapped about 9-times.

That is, we have 13-times more sensitivity in the phase-sum $\varphi_s(x, y)$ compared to the non-wrapped phase-difference $\varphi_D(x, y)$. Figure 5 shows the unwrapped phase-sum $\varphi_s(x, y)$ taking as first estimation the non-wrapped $\varphi_D(x, y)$.

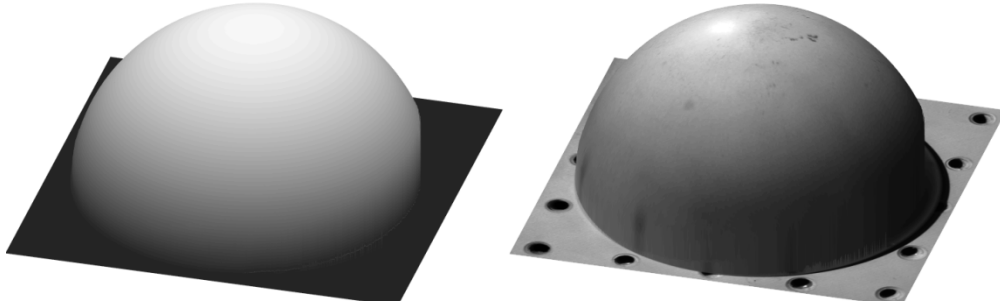


Fig.5. Three-dimensional (3D) digital rendering of the recovered unwrapped phase-sum of the spheric solid. The left-side shows the gray-coded phase-sum, while on the right-side shows the phase-sum with the solid's photograph as texture.

In Fig. 6 we show a central phase-cut of $\varphi_D(x, y)$ and $\varphi_S(x, y)$ to gauge the different amounts of degrading phase-noise.

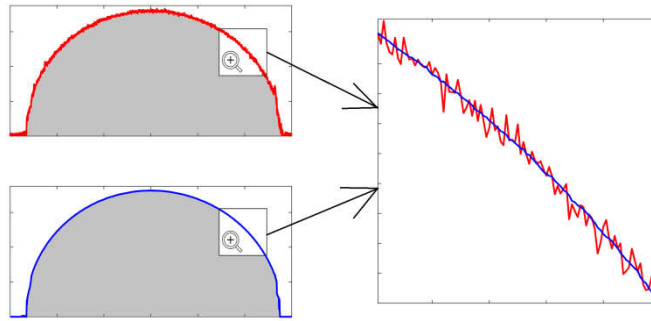


Fig. 6. A central-cut of the digitized spherical cap. The red trace is the phase-difference and the blue trace is the unwrapped phase-sum. The blue trace has significant lower phase-noise.

In the zoomed-in detail one may see the difference in phase-noise amplitude corresponding to the noisier phase-difference in red than the blue phase-sum.

6.2 A fluorescent spiral light bulb

Figure 7 shows our next object a spiral fluorescent lamp. This is a regular photography not a digital rendering.



Fig. 7. Regular Photography (not 3D rendering) of a spiral fluorescent lamp under analysis.

Figure 8 shows phase-shifted linear-fringes with low and high carriers. The upper row carrier is $u_1 = 2\pi / 9$ radians/pixel, while the lower row carrier is $u_2 = 2\pi / 8$ radians/pixel.

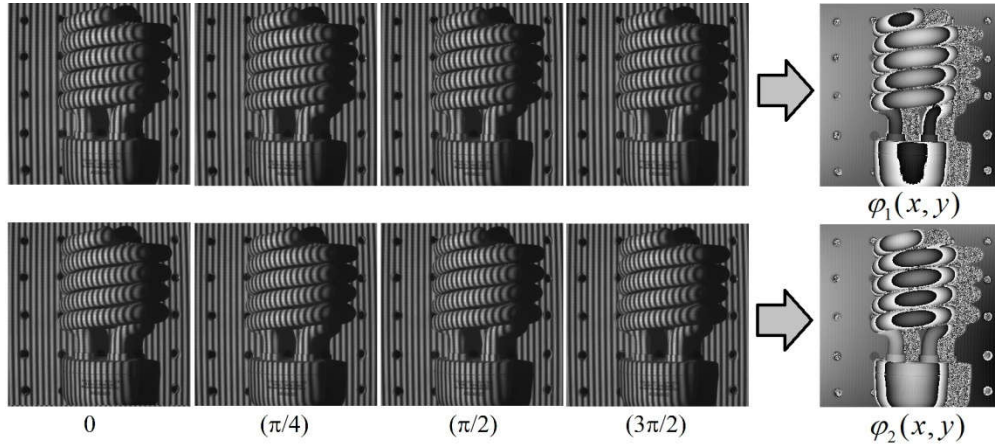


Fig. 8. The spiral lamp illuminated by two close carrier-frequency fringes. The lower carrier fringes are shown in the first row, while the higher carrier fringes are shown in the second row. Their 4-step PSA demodulated wrapped phase are shown at the right column.

Figure 9 shows the phase-difference $\varphi_D(x, y)$ and phase-sum $\varphi_S(x, y)$ of the two sensitivities demodulated phase-maps in Fig. 9.

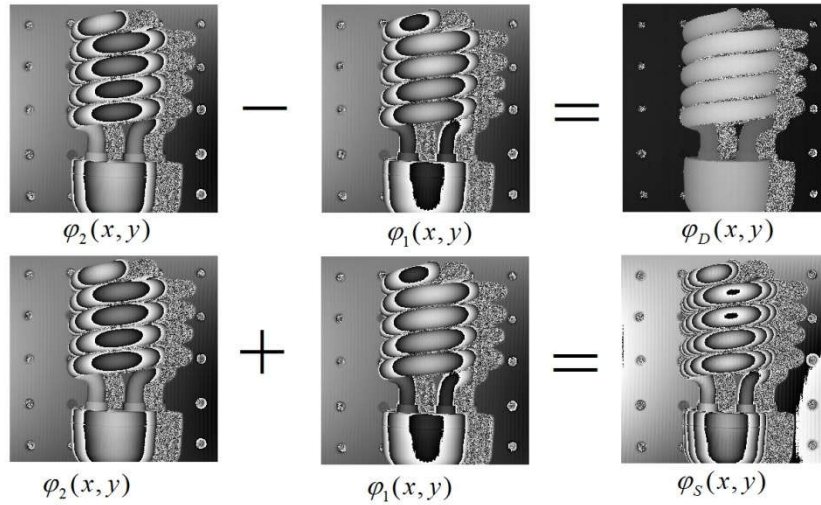


Fig. 9. The upper row shows the non-wrapped phase-difference while the lower row shows the highly wrapped phase-sum. The phase-sum has much higher sensitivity, so it is highly wrapped.

The sensitivity gain G in the spiral-lamp case is given by,

$$G = \frac{u_1 + u_2}{|u_1 - u_2|} = \frac{(2\pi/8 + 2\pi/9) \text{ Radians / Pixel}}{|2\pi/8 - 2\pi/9| \text{ Radians / Pixel}} = 17, \quad (18)$$

That is, we have 17-times more sensitivity in the phase-sum $\varphi_S(x, y)$ compared to the phase-difference $\varphi_D(x, y)$.

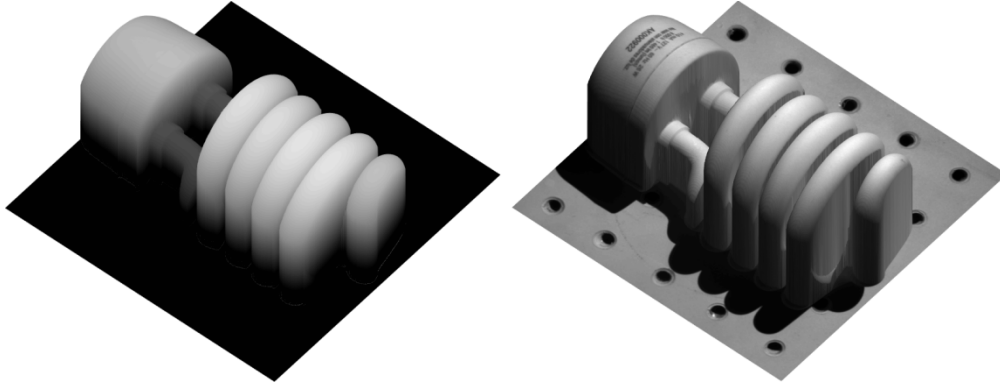


Fig. 10. Digital rendering of the recovered unwrapped super-sensitive phase-sum. The left-side rendering is gray-coded phase. For the right-side we used its photograph as rendering texture.

Figure 10 shows the unwrapped super-sensitive phase-sum.

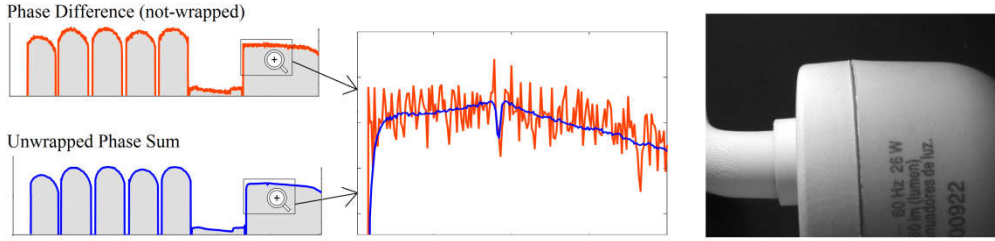


Fig. 11. Comparison of the SNR between the phase-difference (in red), and the super-sensitive phase-sum (in blue). We have zoomed-in to clearly see the depression at the joining of the two plastic pieces shown in the photograph-detail.

Figure 11 shows two phase-cuts of the digitized spiral fluorescent lamp. In the far right a regular zoom-in photograph is shown to see the joint between these two plastic pieces. This joint depression is hardly seen in the red-graph because it is immersed in measuring noise.

7. SNR for high-carrier frequency single and phase-sum profilometry

Before summarizing, we comment another widely used dual-wavelength profilometry strategy [24,25]. This consist of using a very-low carrier u_{Low} (*i.e.* 512 pixels/period) to obtain absolute phase, plus a very-high one $u_{High} = \pi - |\varepsilon|$ ($\varepsilon \approx 0$) to detect fine surface details. The absolute-phase $\varphi_{Low} = u_{Low} \tan(\theta)h$ is used to unwrap $\varphi_{High} = u_{High} \tan(\theta)h$ [24,25]. The unwrapped phases for single and phase-sum high-carrier linear fringes are,

$$\begin{aligned} \varphi_{High} &= u_{High} \tan(\theta)h; \\ \varphi_1 + \varphi_2 &= (u_1 + u_2) \tan(\theta)h. \end{aligned} \quad (19)$$

Assuming that $u_{High} = (u_1 + u_2) / 2$, thus $u_1 + u_2 = 2u_{High}$, and the phase-sum φ_S has twice the sensitivity of φ_{High} ,

$$\frac{\varphi_S}{\varphi_{High}} = \frac{u_1 + u_2}{u_{High}} = 2. \quad (20)$$

And the SNR gain between $(\varphi_1 + \varphi_2)$ and φ_{High} is,

$$\frac{\text{SNR}(\varphi_1 + \varphi_2)}{\text{SNR}(\varphi_{\text{High}})} = \left(\frac{u_1 + u_2}{u_{\text{High}}} \right)^2 = (2)^2 = 4. \quad (21)$$

That is, the SNR for $\varphi_s = \varphi_1 + \varphi_2$ is four times higher than projecting a single fringe-pattern with carrier $u_{\text{High}} = (u_1 + u_2) / 2$; $u_{\text{High}} = \pi - |\varepsilon|$. Therefore the synthetic phase-sum doubles the sensitivity and quadruple the SNR with respect to projecting a single high-frequency fringe-pattern. Therefore there is a clear advantage of using two high-carrier fringes for the same total number of fringe patters; assuming four phase-shifted fringes to obtain $\varphi_{\text{Low}} = u_{\text{Low}} \tan(\theta)h$ plus another four to obtain $\varphi_{\text{High}} = u_{\text{High}} \tan(\theta)h$. This brief analysis was included following a useful suggestion of a reviewer..

8. Summary

We have presented a general mathematical theory for super-sensitivity two-wavelength phase-metrology. In particular we have presented close-form formulae to quantify the SNR and error-free phase-unwrapping for the super-sensitive phase-sum. In particular we have applied this general two-wavelength metrology theory to fringe-projection profilometry. This profilometry method uses linear fringe-patterns with close-sensitivity $\varphi_1 \approx \varphi_2$. Then we compute $\varphi_D = \varphi_2 - \varphi_1$ and $\varphi_s = \varphi_1 + \varphi_2$; being the sensitivity between $\{\varphi_1, \varphi_2\}$ close enough so their difference is non-wrapped *i.e.* $(\varphi_2 - \varphi_1) \in (-\pi, \pi)$. In contrast the super-sensitivity $\varphi_s = \varphi_1 + \varphi_2$ is highly wrapped. Finally we adapted our previous [24,25] phase-unwrapper to unwrap $\varphi_s(x, y)$ error-free directly from $\varphi_D(x, y)$, using a single formula (Eqs. (12)).

As far as we know, the only previous studies [28,29,31] that use $\varphi_s = \varphi_1 + \varphi_2$ and $\varphi_D = \varphi_2 - \varphi_1$ do not contain closed-form mathematical formulae for the SNR of $\{\varphi_s, \varphi_D\}$, neither a mathematical formula for *error-free* unwrapping for $\varphi_s = \varphi_1 + \varphi_2$. Here in contrast, we present closed-form formulae for the SNR of $\{\varphi_1 + \varphi_2, \varphi_1 - \varphi_2\}$, and to unwrap φ_s^W without errors. At the risk of being repetitive, in [28-31] no mathematical analysis and closed-form formulas are provided for: the SNR of $\{\varphi_D, \varphi_s\}$, and for unwrapping φ_s^W without errors. Just specific numerical/experimental examples were displayed [28-31]. However, we know that experimental/numerical demonstrations and/or plausible conjectures, as numerous as they might be, never substitute rigorously obtained mathematical formulae.

Acknowledgments

The authors acknowledge Cornell University for supporting the e-print open repository arXiv.org, and the permission granted by the Optical Society of America which allows uploading submitted manuscripts to arXiv.org. We thank a reviewer for calling our attention to the recent work by Di et al. work [29]. Using Google Scholar we tracked down its two related works [28,31].